Supporting Information

Microscopic Droplet Formation and Energy Transport Analysis of Condensation on Scalable Superhydrophobic Nanostructured Copper Oxide Surfaces

GuanQiu Li, Mohamed H. Alhosani, ShaoJun Yuan, HaoRan Liu, Amal Al Ghaferi, TieJun Zhang*

Department of Mechanical and Materials Engineering, Masdar Institute of Science and Technology, P. O. Box 54224, Abu Dhabi, UAE
* Corresponding author: tjzhang@masdar.ac.ae

S1 Supporting Video Legends

Supporting Video S1. Single droplet growth process on Sample 1 captured by ESEM. The video was captured at 0.95 fps and is played back at 10 fps. The field of view is 25.4 μm× 21.9 μm.

Supporting Video S2. Microscale droplet growth on Sample 1 captured by ESEM. The video was captured at 0.95 fps and is played back at 10 fps. The field of view is 127 μm× 109.6 μm.

Supporting Video S3. Microscale droplet growth on Sample 2 captured by ESEM. The video was captured at 0.95 fps and is played back at 10 fps. The field of view is 127 μm× 109.6 μm.

S2 Fabrication

S2.1 Pretreatment. Each copper tab was cleaned in an ultrasonic bath with acetone, ethanol, IPA, and de-ionized (DI) water (Sigma-Aldrich) for 15 minutes each to remove the organic contaminants on the surface. The substrate was then dipped into a 2 mol/L hydrochloric acid (37%, Sigma-Aldrich) solution for 20 minutes to remove the existing oxide, then rinsed with DI water and dried with pure nitrogen.

S2.2 Anodization. The growth of $Cu(OH)_2$ nanoneedle arrays was carried out at a constant temperature (10 ℃) and in a typical electrolyte (KOH solutions) with two different concentrations (2.0 mol/L for Sample 1 and 1.0 mol/L for Sample 2). The cleaned copper foil was used as the working electrode (anode), which had a surface area of ~ 4.5 cm^2. The counter electrode (cathode) was a type 304 stainless steel foil with surface area ~ 4.5 cm^2. The distance between the anode and cathode is fixed at 2 cm during anodization. The growth of $Cu(OH)_2$ nanoneedle arrays was an electrochemical process and the chemical reactions of anode and cathode are described as,[1]

Anode: $$Cu - 2e^- \rightarrow Cu^{2+},\ Cu^{2+} + 2OH^- \rightarrow Cu(OH)_2\downarrow \quad (S1)$$

Cathode: $$2H^+ + 2\ e^- \rightarrow H_2\uparrow \quad (S2)$$

During anodization, the KOH solutions should be deaerated by a dry nitrogen stream to get rid of oxygen in the electrolyte. The anodization current between anode and cathode was set to be constant (3 mA) by Autolab PGSTAT 100 (Metrohm Autolab Instruments), and the temperature of the electrolyte was maintained at 10 ℃ during anodization. The anodization conditions for the two samples are summarized in Table S1.

Table S1 Anodizatioin conditions for the two CuO nanostructured surface

Anodization condition	Electrolyte concentration	Anodization current	Temperature	Anodization time
Sample 1	2 mol/L	3 mA	10 ℃	40 minutes
Sample 2	1 mol/L	3 mA	10 ℃	40 minutes

S2.3 Crystallization. After anodization, samples were heated to 150℃ for 3 hours to complete dehydration. Then the temperature was raised to 200 ℃ and kept for another 3

hours to promote crystallization. Thus, copper oxide (CuO) nanoneedle arrays were formed on the substrates with stable and robust structures.[2]

S2.4 Silanization. For Sample 1, the nanostructured CuO arrays were functionalized using self-assembly deposition of a fluorosilane. Briefly, 1gram of 1H, 1H, 2H, 2H-perfluorodecyltriethoxysilane (FAS-17, Sigma-Aldrich) and 99 grams of ethanol were mixed together for 3 hours under continuous stirring to prepare the fluoroalkylsilane solution under vacuum conditions. Thereafter, the as-prepared nanoneedle CuO-structured sample was immersed in the fluoroalkylsilane solution for 12 hours at ambient temperature. Resulting superhydrophobic samples were rinsed in ethanol and dried with a clean nitrogen stream.

For Sample 2, prior to silane deposition, the nanostructured CuO was oxygen plasma cleaned for 30 minutes to remove organic contaminants and increase the surface temperature. Once cleaned, Sample 2 was functionalized using chemical vapor deposition of a fluorinated silane (trichloro (1H,1H,2H,2H-perfluorooctyl) silane, Sigma-Aldrich) and placed in a vacuum desiccator (VWR International) with a small amount (~ 0.1 milliliter) of liquid silane. The desiccator was evacuated by a vacuum pump for 15 minutes and the sample will be kept in vacuum for 30 minutes. The samples were rinsed in ethanol and DI water and dried with a clean nitrogen stream.

S3 Charaterization.

Small angle X-ray diffraction (XRD) spectrums of the nanoneedle CuO-covered copper surface with different anodization time and same electrolyte concentration 2 mol/L were obtained, and the results are shown in Figure S3.1. The formation of crystalline CuO on the

anodized surface can be deduced from the appearance of two additional diffraction peaks with 2θ at 35.8 and 38.6, which are attributable to the monoclinic structure CuO (JCPDS 05-0661). Since only a small amount of CuO nanoneedles grows on the copper substrates after 5 min of anodization, the crystalline CuO diffraction peaks in the XRD spectrum is undetectable, which further supports the formation of nanoneedle CuO by anodization rather than reacting with O_2 when the copper was exposed in the air, and 5 min anodization time was insufficient to obtain adequate nanoneedle arrays.

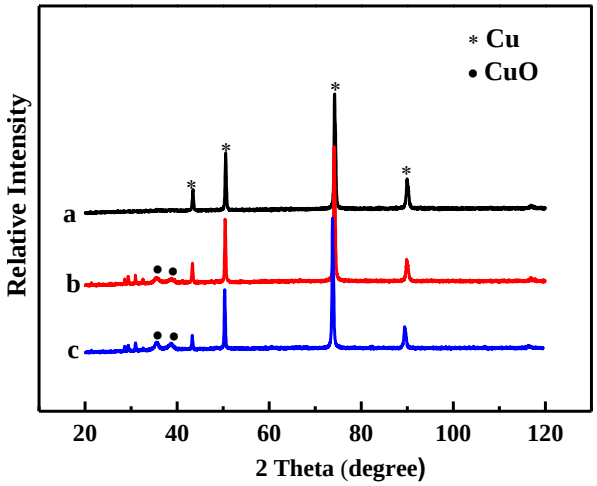

Figure S3.1 XRD spectrums of the anodized copper substrate (2 mol/L) with anodization time of (a) 5min, (b) 25min and (c) 40min

Figure S3.2 shows the EDS analysis of anodized CuO surfaces under 40 minutes deposition time and 2.0 mol/L electrolyte concentration. Quantitative information for each element on Sample 1 before and after silanization is shown in Figs. S3.2 (a) and S3.2 (c). The results of EDS mapping are shown in Figs. S3.2 (b) and S3.2 (d). White base with nanoneedle shape is copper, while other colors represent different elements (Red: Oxygen, Blue: Silicon, Green: Fluorine). EDS maps confirm that the anodized CuO nanoneedles after the anodization and silanization process covered the whole surface of the copper substrate uniformly.

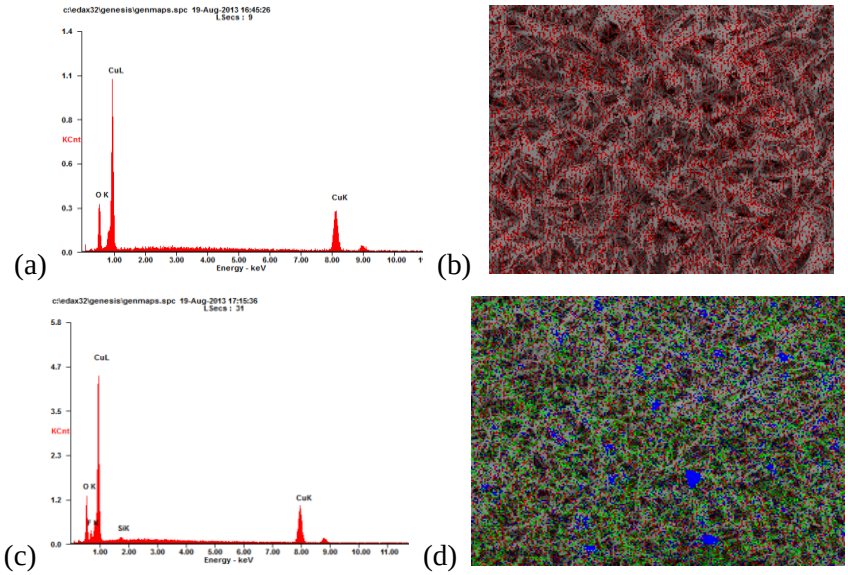

Figure S3.2 (a) Extracting quantitative information for CuO surface before silanization; (b) EDS mapping for CuO surface before silanization; (c) Extracting quantitative information for CuO surface after silanization; (d) EDS mapping for CuO surface after silanization.

The surface microstructure and water contact angle profiles on the superhydrophobic nanoneedle CuO-covered surface were characterized by SEM and water contact angle measurement, respectively, and the results were shown in Figure S3.3. In comparison with the anodized copper surface with nanoneedle CuO arrays, no significant difference can be observed on the fluorosilanized superhydrophbic copper surfaces. This result is consistent with the fact that a monolayer of fluorosilane was immobilized on the nanoneedle CuO arrays by self-assembly reaction. It has been reported that the thickness of a silane monolayer is less than 1.5 nm.[3,4] The static water contact angle of the flurosilanized nanoneedle CuO array-covered copper is as high as around 161^{o} (Fig. S2.3 a′), indicative of the superhydrophobicity of the copper surface. The optical images of water droplets further suggest uniform surface superhydrophobicity of the fluorosilanized nanoneedle CuO array-covered copper (Fig. S2.3 a″). AFM measurements were taken to get the structure

height distribution and actural surface area for calculating the roughness factor distribution, which are shown in Figure S3.4. In addition, the 3D images of the irregular CuO nanostructures are shown in Figure S3.4.

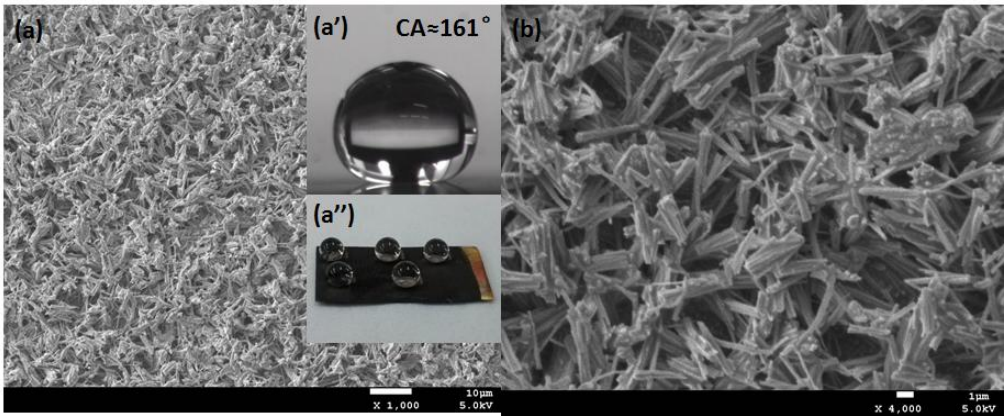

Figure S3.3 SEM images of the fluorosilanized nanoneedle CuO-covered copper surface at (a) low (1000×) and (b) high (4000×) magnifications, Insets (a′) and (a″) represents contact angle profile of a water droplet and the optical image of water droplets on the as-prepared superhydrophobic surface, respectively.

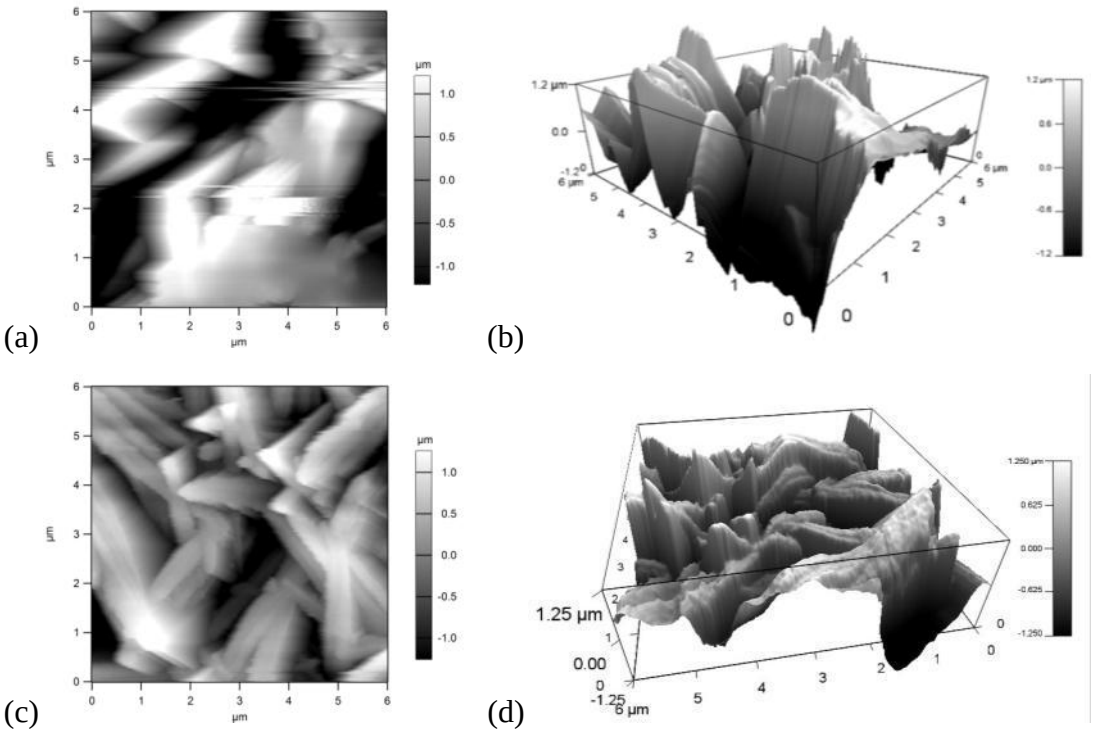

Figure S3.4 (a) Height distribution from AFM and (b) 3D images from AFM, for Sample 1; (c) Height distribution from AFM and (d) 3D images from AFM, for Sample 2;

S4 Local energy barriers for initial growth beyond the structures

After the microscale droplet forms on the nanostructured surface, the droplet grows to occupy the volume within the nanostructures and encounters two distinct energy barriers associated with the top and side of the droplet. We approximate the magnitude of the two energy barriers by considering the energy cost for an incremental increase in volume in each direction. The droplet is bound by energy barriers at the side ($\triangle E_s$) and at the top ($\triangle E_t$) of the CuO nanoneedles as shown in Figure S4.1. It is assumed that the initial droplet shape is spherical cap beyond the structures and cylinder within the structures, and the liquid volume changes within and beyond the structures of the droplet are equal ($\triangle V_s = \triangle V_t$).

$$\mathrm{d}V_t = \frac{\pi}{3}(R+\mathrm{d}R)^3[2-3\cos(\theta+\mathrm{d}\theta)+\cos^3(\theta+\mathrm{d}\theta)] - \frac{\pi}{3}R^3[2-3\cos\theta+\cos^3\theta] \quad \text{(S3)}$$

$$\mathrm{d}V_s = \pi[(b+\mathrm{d}b)^2 - b^2]h_n(1-\varphi) \quad \text{(S4)}$$

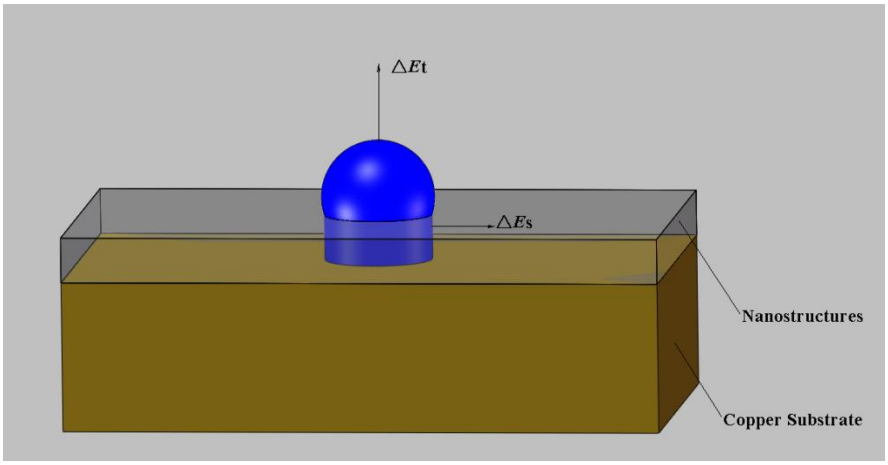

Figure S4.1 Two respective energy barriers for initial droplet growth beyond the structures

It is assumed that the base radius of the droplet remain the same for the droplet growth beyond the structures ($b = R\sin\theta = (R+\mathrm{d}R)\sin(\theta+\mathrm{d}\theta)$), while the base radius has an increment (db) when the droplet grows within the structures. As a result, a relation between the change in major radius (dR) and the change in contact angle (dθ) can be written[5]

$$\mathrm{d}R = -R\cot\theta\,\mathrm{d}\theta \tag{S5}$$

Combining Eq.(S5) and $\mathrm{d}V_\mathrm{t} = \mathrm{d}V_\mathrm{s}$, a relation between d$\theta$ and db can be found,

$$2h_n(1-\varphi)\mathrm{d}b = R^2\left(\frac{1-\cos\theta}{\sin\theta}\right)^2\mathrm{d}\theta \tag{S6}$$

In the case of overcoming the energy barrier beyond the structures, the energy change during this process can be expressed,

$$\mathrm{d}E_\mathrm{t} = [2\pi(R+\mathrm{d}R)^2(1-\cos(\theta+\mathrm{d}\theta)) - 2\pi R^2(1-\cos\theta)]\gamma_\mathrm{lv} \tag{S7}$$

For the energy barriers within the structures, it can be expressed as

$$\mathrm{d}E_\mathrm{s} = [2\pi(b+\mathrm{d}b) - 2\pi b]h\gamma_\mathrm{lv} - [\pi(b+\mathrm{d}b)^2 - \pi\mathrm{b}^2]r_\mathrm{f}(\gamma_\mathrm{sl}-\gamma_\mathrm{sv}) \tag{S8}$$

Comparing the ratio of the two respective energy barriers and combine Eq.(S6), we find

$$E^* = \frac{\Delta E_\mathrm{t}}{\Delta E_\mathrm{s}} = \frac{2h_n(1-\varphi)\sin\theta_n}{h_n - br_\mathrm{f}\cos\theta_\mathrm{a}} \tag{S9}$$

Once the top energy barrier is relatively small (E^*<1), the droplet grows beyond the structures, while for E^*>1, the droplet favors wetting within the structures. In addition, from Eq. (S9), the relation between E^* and h, b, r_f, φ can be found.

S5 Pinning barriers for droplet growth

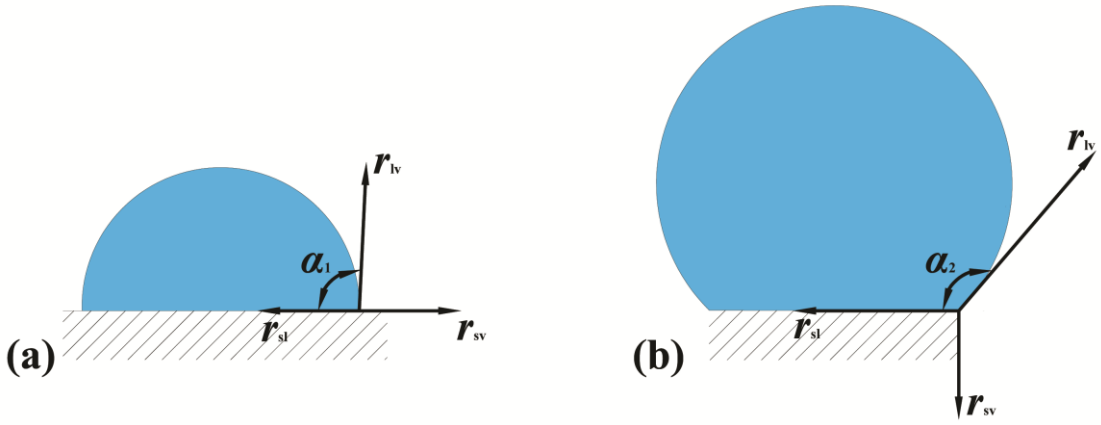

Figure S5.1 Edge effect of a single droplet

The interfacial surface tensions at the edge of a surface are the key to understand the microscale droplet growth at early stage of condensation. As shown in Figure S5.1(a), a force balance can be achieved when a droplet is formed on a smooth surface. However, when the droplet reaches the edge of a surface, the solid-vapor surface tension changes its direction from horizontal to vertical. Based on the force balance in this case, the droplet will be pinned at the edge until a threshold contact angle is reached, which can be obtained from the new force balance in Fig. S5.1(b). Similar approach can be used for the local droplet growth model on nanostructured surfaces.

When E^*>1, the structures are fully wetted. It is assumed that, the initial droplet shape is spherical cap beyond the structures and cylinder within the structures, same as Figure S4.1. After E^*<1, the droplets start to grow beyond the nanostructures. In order to predict the microscale droplet growth behavior that give rise to the observed droplet morphologies in Figures 1(e) and 1(f), the interfacial surface tensions at the edges of the nanoneedles are analyzed to calculate the threshold contact angle at different stages shown in Figure 4. The force balances comprise of the balance on the CuO nanoneedles and the balance between the CuO nanoneedles. The contact line between the droplet and nanoneedles can be divided into two parts: the solid (CuO nanoneedles) and the liquid (between the nanoneedles). The percentage of the two respective parts can be expressed as[6]

$$f_1 = \frac{\left(\frac{\pi b}{l} - 1\right) \times \frac{\pi d}{2}}{2\pi b}, f_2 = 1 - f_1 \tag{S10}$$

As shown in Figure 4, three interfacial surface tensions can be found on the nanoneedles; while there are only two interfacial surface tensions on the liquid between the nanoneedles. We assume that the average inclination angles of one half of the nanoneedles are θ_n and those

of the other half are π-θ_n. θ_n can be calculated from the average length and average height of the nanoneedles. Considering the force balances on the nanoneedles and between the nanoneedles, the first threshold contact angle (for stage 1 shown in Figure 4(a)) was calculated

$$\begin{aligned}&\frac{1}{2}\times[(\gamma_{sv}-\gamma_{sl})f_1\sin\theta_n+\gamma_{lv}(f_1+f_2)\sin\alpha_1-\gamma_{lv}f_2]\\&+\frac{1}{2}\times[(\gamma_{sv}-\gamma_{sl})f_1\sin(\pi-\theta_n)+\gamma_{lv}(f_1+f_2)\sin\alpha_1-\gamma_{lv}f_2]=0\end{aligned}\tag{S11}$$

Then we can solve for the first threshold contact angle α_1 (for stage 1 shown in Figure 4(a)),

$$\sin\alpha_1=f_2+f_1\cos\theta_a\sin\theta_n\tag{S12}$$

The second threshold contact angle (for stage 2 in Figure 4(b)) can be achieved when the interface of the droplet contacts with the surrounding nanoneedles without complete wetting of the intervening gap between the nanoneedles. Therefore, the direction of liquid-vapor interfacial surface tension shown inside the red circle in Figure 4(b) is no longer vertical. This direction is assumed to have an angle same as α_1. Then the force balance for the second threshold contact angle (for stage 2 in Figure 4(b)) can be expressed as,

$$\begin{aligned}&\frac{1}{2}\times[(\gamma_{sv}-\gamma_{sl})f_1\sin\theta_n+\gamma_{lv}(f_1+f_2)\sin\alpha_2-\gamma_{lv}f_2\sin\alpha_1]\\&+\frac{1}{2}\times[(\gamma_{sv}-\gamma_{sl})f_1\sin(\pi-\theta_n)+\gamma_{lv}(f_1+f_2)\sin\alpha_2-\gamma_{lv}f_2\sin\alpha_1]=0\end{aligned}\tag{S13}$$

Then α_2 can be expressed as,

$$\sin\alpha_2=f_2\sin\alpha_1+f_1\cos\theta_a\sin\theta_n\tag{S14}$$

Similarly, we can get the threshold contact angle for depinning stage i (α_i)

$$\sin\alpha_i=f_2\sin\alpha_{i-1}+f_1\cos\theta_a\sin\theta_n\tag{S15}$$

S6 Prediction for droplet jumping

At the dropwise condensation mode, the droplets move and take away the heat[7] more effectively when their sizes approach the capillary length (2.7 mm for water in air) . On the other hand, the jumping droplets are able to quickly transfer the heat between the solid surface and the ambient even though the droplet size is much smaller than the capillary length[8]. In fact, droplet jumping occurs due to the coalescence of droplets with radius ranging from several microns to hundreds of microns[9-10].

Droplet jumping was observed during the *in-situ* ESEM condensation experiment and the results are summarized in Table 3**.** The model proposed by F. C. Wang et al.[9] have been extended to the coalescence of two droplets with different sizes. Our improved model is able to estimate the kinetic energy of the coalescent droplet just after it leaves the solid surface (θ = 180°). Considering the viscous dissipation losses, work of adhesion while neglecting potential energy, the kinetic energy of the coalescent droplet from two droplets can be calculated[11],

$$E_{\mathrm{k}} = \Delta E_{\mathrm{s}} - E_{\mathrm{vis}} - E_{\mathrm{w}} \tag{S16}$$

The surface energy change ΔE_{s} ,[12] viscous dissipation losses E_{vis},[10] and work of adhesion E_{w} [13] can be calculated as follow,

$$\Delta E_{\mathrm{s}} = \pi\gamma_{lv}(R_1^2 + R_2^2)(2 - 2\cos\theta - C(f)sin^2\theta) - 4\pi\gamma_{lv}(R_1^3 + R_2^3)^{\frac{2}{3}} \tag{S17}$$

$$E_{\mathrm{vis}} = 36\pi\mu\left(R_1^{\frac{3}{2}} + R_2^{\frac{3}{2}}\right)\sqrt{\frac{\gamma_{\mathrm{lv}}}{\rho_{\mathrm{w}}}} \tag{S18}$$

$$E_{\mathrm{w}} = \gamma_{\mathrm{lv}}(1 + \cos\theta)A_{\mathrm{sl}} \tag{S19}$$

For partially wetting droplets, the coefficient $C(f)$ can be obtained from the minimum of surface energy,[7]

$$C(f) = [r_f m + (1-m)\varphi]\cos\theta_E - (1-m)\cdot(1-\varphi) \quad \text{(S20)}$$

m is the percentage of liquid volume within the nanostructures over total volume within the nanostructures. When m=0, the droplet is in Cassie state; and when m=1, the droplet is in Wenzel state.

A_{sl} is the percentage of trapped liquid within nanostructures, which can be calculated below,

$$A_{sl} = \pi R^2 \sin^2\theta (m r_f + (1-m)\varphi) \quad \text{(S21)}$$

R is the radius of the droplet.

Combined Eqs. S17-S21, the kinetic energy of the coalescent droplet can be found

$$\begin{aligned} E_k = &\left[\pi\gamma_{lv}(R_1^2+R_2^2)(2-2\cos\theta - C(f)sin^2\theta) - 4\pi\gamma_{lv}(R_1^3+R_2^3)^{\frac{2}{3}}\right] \\ &-36\pi\mu\left(R_1^{\frac{3}{2}}+R_2^{\frac{3}{2}}\right)\sqrt{\frac{\gamma_{lv}}{\rho_w}} - \gamma_{lv}(1+\cos\theta_E)\pi(R_1^2+R_2^2)\sin^2\theta(m r_f + (1-m)\varphi) \end{aligned} \quad \text{(S22)}$$

Then the jumping velocity can then be found by,

$$v = \left[\begin{array}{l} \frac{3\gamma_{lv}}{2\rho}\left(\frac{R_1^2+R_2^2}{R_1^3+R_2^3}\right)(2-2\cos\theta - C(f)sin^2\theta) - \frac{6\gamma_{lv}}{\rho}\frac{1}{\sqrt[3]{R_1^3+R_2^3}} - 54\mu\sqrt{\frac{\gamma_{lv}}{\rho^3}} \\ \quad \times\left(\frac{R_1^{\frac{3}{2}}+R_2^{\frac{3}{2}}}{R_1^3+R_2^3}\right) - \frac{3\gamma_{lv}}{2\rho}(1+\cos\theta_E)\left(\frac{R_1^2+R_2^2}{R_1^3+R_2^3}\right)\sin^2\theta(m r_f + (1-m)\varphi) \end{array}\right]^{\frac{1}{2}} \quad \text{(S23)}$$

S7 Global droplet growth model

The predicted growth of the microscale droplet formed on the structured surface, was obtained by modifying the model developed by Umur et al.[14] and Milikovic et al.,[4] considering the irregular nanostructures and liquid volume change within the nanostructures. For the microscale droplets, the dominant mode of droplet growth is due to the direct accommodation of vapor molecules at the droplet interface.[16] The thermal resistances between the water vapor and the substrate can be calculated as follows,

$$R_{\mathrm{i}} = \frac{1}{2\pi R^2 h_{\mathrm{i}}(1-\cos\theta)} \tag{S24}$$

$$h_{\mathrm{i}} = \frac{2\alpha}{2-\alpha}\frac{1}{\sqrt{2\pi R_g T_{\mathrm{S}}}}\frac{h_{\mathrm{fg}}^2}{\nu_g T_{\mathrm{S}}} \tag{S25}$$ [15]

$$R_{\mathrm{d}} = \frac{\theta}{4\pi R k_{\mathrm{w}} \sin\theta} \tag{S26}$$

$$R_{\mathrm{WN}} = \frac{1}{\pi R^2 k_{\mathrm{SC}} \sin^2\theta}\left[\frac{k_{\mathrm{N}}\varphi r_{\mathrm{f}}}{\delta_{\mathrm{SC}} k_{\mathrm{N}} + r_{\mathrm{f}} h k_{\mathrm{SC}}} + \frac{k_{\mathrm{W}}(1-\varphi)m_{\mathrm{i}}}{\delta_{\mathrm{SC}} k_{\mathrm{W}} + h_n k_{\mathrm{SC}}}\right]^{-1} \tag{S27}$$

For the microscale droplets, internal droplet convection was neglected in the model and therefore conduction is the primary mode of heat transfer through the droplet.[17-18] The condensation coefficient (α) in Eq. (S25) is the ratio of vapor molecules that will be captured by the liquid phase to the total number of vapor molecules reaching the liquid surface (ranging from 0 to 1). α is assumed to be 0.9, which is appropriate for clean environments [15], such as ESEM.

Considering all the thermal resistances, heat transfer rate, q, through a condensing droplet is,

$$q = \frac{\Delta T - \Delta T_{\mathrm{C}}}{\sum R_{\mathrm{j}}} \tag{S28}$$

$$\sum R_{\mathrm{j}} = R_{\mathrm{i}} + R_{\mathrm{d}} + R_{\mathrm{WN}} \tag{S29}$$

$$\Delta T_{\mathrm{C}} = \frac{R_{\min}}{R}(T_{\mathrm{sat}} - T_{\mathrm{S}}) = \frac{2T_{\mathrm{sat}}\sigma}{R h_{\mathrm{fg}} \rho_{\mathrm{w}}} \tag{S30}$$

It is worth noting that the different surface roughness needs to be considered for calculating the conduction resistance of liquid within the nanostructures. The nanostructures cannot be fully wetted by the liquid and the liquid volume can be predicted by the local droplet growth model shown in Section 3.1.2. The percentage of liquid volume over total volume within the nanostructures can be obtained (m_1- m_4 for stage 4 to stage 1 and m_5 for stage 0 (fully wetting), as shown in Figure 4). Because of the heterogeneity of the CuO nanostructures, the entire surfaces cannot have a uniform apparent contact angle. Roughness distributions of Sample 1 and Sample 2 are obtained by AFM data shown in Figure S3.4.[19]

The percentage of different surface roughness shown in Table 2 can be obtained (n_1- n_4 for stage 4 to stage 1 and n_5 for stage 0 (fully wetting), $\sum n_{\mathrm{i}} = 1$). In addition, the apparent contact angles used in the global droplets growth model can be predicted by the results shown in Figure 4. Combining Eqs. (S28)-(S30),

$$q = \sum_{\mathrm{i}=1}^{5} \frac{n_{\mathrm{i}} \times \pi R^2 \Delta T \left(1 - \frac{R_{\min}}{R}\right)}{\frac{1}{2h_{\mathrm{i}}(1-\cos\theta)} + \frac{\theta R}{4k_{\mathrm{w}}\sin\theta} + \frac{1}{k_{\mathrm{SC}}\sin^2\theta}\left[\frac{k_{\mathrm{N}}\varphi r_{\mathrm{f}}}{\delta_{\mathrm{SC}}k_{\mathrm{N}} + h_n k_{\mathrm{SC}} r_{\mathrm{f}}} + \frac{k_{\mathrm{W}}(1-\varphi)m_{\mathrm{i}}}{\delta_{\mathrm{SC}}k_{\mathrm{W}} + h_n k_{\mathrm{SC}}}\right]^{-1}} \quad \text{(S31)}$$

In addition, considering influence of electron beam in ESEM chamber, the droplet growth rate can be obtained as follows,

$$q - q_{\mathrm{beam}} \times \eta_{\mathrm{u}} \times \eta_{\mathrm{f}} = \rho_{\mathrm{w}} h_{\mathrm{fg}} \frac{\mathrm{d}V}{\mathrm{d}t} \quad \text{(S32)}$$

$$\frac{\mathrm{d}V}{\mathrm{d}t} = \left[\pi R^2(2 - 3\cos\theta + \cos^3\theta) + 2\pi R \sin^2\theta\,(1-\varphi)h_{\mathrm{n}}\right]\frac{\mathrm{d}R}{\mathrm{d}t} + \left[\pi R^3 \sin^3\theta + 2\pi R^2 \sin\theta\cos\theta\,(1-\varphi)h_{\mathrm{n}}\right]\frac{\mathrm{d}\theta}{\mathrm{d}t} \quad \text{(S33)}$$

The heating effect of the electron beam can be calculated from the primary beam energy from the electron gun in ESEM chamber (q_{beam}) and the efficiencies (η_{u} and η_{f}).[20-21] q_{beam} can be obtained through the initial beam potential and beam current. η_{u} shows how many electrons are not scattered before they reach the sample surface, under different pressure and working distance. η_{f} means how many effective electrons are focused after they pass through the water vapor. Based on the experimental conditions, η_{u} =23% and η_{f} =3%.[20-21]

Supplemental References

(1) Wu, X.F.; Bai, H.; Zhang, J.X.; Chen, F.E.; Shi, G.Q. Copper Hydroxide Nanoneedle and Nanotube Arrays Fabricated by Anodization of Copper. *J. Phys. Chem. B* **2005**, 109, 22836-22842.

(2) Wu, X. F.; Shi, G. Q. Production and Characterization of Stable Superhydrophobic Surfaces Based on Copper Hydroxide Nanoneedles Mimicking the Legs of Water Striders. *J. Phys. Chem. B* **2006**, 110, 11247-11252.

(3) Love, J. C.; Estroff, L. A.; Kriebel, J. K.; Nuzzo, R. G.; Whitesides, G. M. Self-Assembled Monolayers of Thiolates on Metals as a Form of Nanotechnology. *Chem.*

Rev. **2005**,105, 1103–1169.
(4) Miljkovic, N.; Enright R.; Wang, E.N. Effect of Droplet Morphology on Growth Dynamics and Heat Transfer during Condensation on Superhydrophobic Nanostructured Surfaces. *ACS Nano* **2012**, 6 (2), 1776-1785.
(5) Raj, R.; Enright, R.; Zhu, Y.Y.; Adera, S.; Wang, E.N. Unified Model for Contact Angle Hysteresis on Heterogeneous and Superhydrophobic Surfaces. *Langmuir* **2012**, 28 (45), 15777-15788.
(6) Enright, R.; Miljkovic, N.; Obeidi, A.A.; Thompson, C.V.; Wang, E.N. Condensation on Superhydrophobic Surfaces: The Role of Local Energy Barriers and Structure Length Scale. *Langmuir* **2012**, 28(40), 14424-14432.
(7) Gennes, P.G.D.; Wyart, F.B.; Quere, D. Capillarity and Wetting Phenomena, Drops, Bubbles, Pearls, Waves, Translated by Axel Reisinger, New York: *Springer Science* **2002**, 1-15.
(8) Miljkovic, N; Enright, R.; Nam, Y.; Lopez, K.; Dou, N.; Sack, J.; Wang, E.N. Jumping-Droplet-Enhanced Condensation on Scalable Superhydrophobic Nanostructured Surfaces. *Nano Lett.* **2013**, 13(1), 179-187.
(9) Wang, F. C.; Yang, F.; Zhao, Y. P. Size effect on the coalescence-induced self-propelled droplet. *Appl. Phys. Lett.* **2011**, 98(5), 053112.
(10) Boreyko, J. B.; Chen, C. H. Self-Propelled Dropwise Condensate on Superhydrophobic Surfaces. *Phys. Rev. Lett.* **2009**, 103, 184501.
(11) Liu, T.Q.; Sun, W.; Sun X.Y. Mechanism study of condensed drops jumping on super-hydrophobic surfaces. *Colloids and Surfaces A: Physicochem. Eng. Aspects* **2012**, 414, 366-374.
(12) Marmur, Abraham. Wetting on Hydrophobic Rough Surfaces: To Be Heterogeneous or Not To Be? *Langmuir* **2003**, 19, 8343-8348.
(13) Gao, L.; McCarthy, T.J. Wetting 101 degree. *Langmuir* **2009**, 25(24), 14105–14115.
(14) Umur, A.; Griffith, P., Mechanism of Dropwise Condensation. *J. Heat Trans.* **1965**, 87, 275–282.
(15) Carey, V.P., Liquid-Vapor Phase-Change Phenomena: An Introduction to the Thermophysics of Vaporization and Condensation Processes in Heat Transfer Equipment, New York: 2nd edition, *Taylor and Francis* 2008.
(16) Kaschiev, D. Nucleation: Basic Theory With Applications. *Butterworth Heinemann: Oxford* **2000**.
(17) Tanaka, H.; Tsuruta, T., A Microscopic Study of Dropwise Condensation. *Int. J. Heat Mass Tran.* **1984**, 27, 327-335.
(18) Tam, D.; von Arnim, V.; McKinley, G. H.; Hosoi, A. E., Marangoni Convection in Droplets on Superhydrophobic Surfaces. *J. Fluid Mech.* **2009**, 624, 101-123.
(19) Torregrosa, P. J. R.; Valverde, M. A. R.; Amirfazli, A.; V´ılchez, M. A. C. Factors affecting the measurement of roughness factor of surfaces and its implications for wetting studies. *Colloid Surface A* **2008**, 323, 83–93.
(20) FEI Company, *The Quanta FEG 250 / 450 / 650 User Operation Manual*, 5th Edition, **2010**.
(21) FEI Company, *Quanta Training - X50 series, ESEM mode* **2013**.